18th AIAA Computational Fluid Dynamics Conference, 25-28 Jun 2007, Miami, FL

Statistical Modeling of Rarefied Gas Flows in Microchannels

Seckin Gokaltun*, Peter V. Skudarnov†
Applied Research Center, Florida International University,
10555 W. Flagler St., EC 2100, Miami, FL 33174

Michael C. Sukop‡
Department of Earth Sciences,
Florida International University, PC 344, University Park, 11200 SW 8th Street, Miami, FL 33199

George S. Dulikravich§
Department of Mechanical and Materials Engineering,
Multidisciplinary Analysis, Inverse Design, Robust Optimization and Control (MAIDROC) Lab.,
Florida International University, 10555 W. Flagler St., EC 3474, Miami, FL 33174

Lattice Boltzmann method (LBM) and direct simulation Monte Carlo (DSMC) method are used for analysis of moderate Knudsen number phenomena. Simulation results are presented for pressure driven isothermal microchannel flow at various pressure ratios. Analytical equations for non-linear pressure distribution and velocity profiles along the channel axis are used to verify the present LBM and DSMC results. We conclude that the LBM method can be used as an alternative model to DSMC simulations.

I. Introduction

MICRO Electro Mechanical Systems (MEMS) refer to devices that have characteristic lengths typically of the order of microns[1]. Micro-actuators, micro-turbines, micro-heat exchangers and micro-pumps are some of them. When the characteristic length scale in microsystems become comparable to the mean free path (λ) the flow becomes rarefied and continuum approach fails to predict the characteristics of rarefied gas flows in MEMS devices mainly because the thermodynamic equilibrium is not achieved due to lack of collisions between molecules. The rarefaction of the flow is described using the non-dimensional parameter called Knudsen number given as $Kn = \frac{\lambda}{H}$ where $\lambda = \frac{\kappa T}{P\sigma^2\pi\sqrt{2}}$ is the mean free path and H is the characteristic length. The classification of the flow regimes in terms of Knudsen number can be viewed as:[2]

- $0 < Kn < 0.01$: Continuum regime
- $0.01 < Kn < 0.1$: Slip Flow regime
- $0.1 < Kn < 10$: Transition regime
- $10 < Kn$: Free molecular regime

*Research Assistant, AIAA member.
†Research Scientist, AIAA member.
‡Assistant Professor.
§Professor, AIAA associate fellow.

In continuum and slip flow regime, Navier-Stokes based numerical methods can be used with special treatment for gas-surface interactions to model the gas flow and heat transfer in microsystems[3,4]. However limited applicability of these models and empirical determination of the momentum accomodation constant (σ) for the surface boundary treatment make CFD simulations inpracticle for modeling gas flow in microsystems.

Molecular based modeling can be used to simulate gas flow in MEMS devices for the whole flow regime[1]. In molecular modeling of gas flows the fluid is treated as collection of a huge number of particles sufficient to yield macroscopic properties of the flow. Direct Simulation and Monte Carlo (DSMC) and Lattice-Boltzmann Method (LBM) are statistical approaches to molecular modeling of gas flows. Successful applications of DSMC modeling of gas flows in microchannels were published in the literature.[5–7]

DSMC results for microchannel gas flow in slip and transition regime has been published by Xue et al[5]. Comparison with analytical solutions has shown that the continuum model with slip boundary conditions predicts a higher cross sectional velocity distribution along the microchannel compared to DSMC results in transition regime. Fang and Liou demonstrated DSMC results for micro-poiselle and micro-couette flow for straight and constricted microchannels in the slip flow regime[6]. Their comparison with Navier-Stokes based analytical solutions were in good agreement. The standard DSMC method has been extended by Wang and Li for non-ideal gas flows in microchannels[7]. In their simulations the DSMC method was modified with a Boltzmann algorithm and van der Walls equation was used as the equation of state.

LBM was also proved to give accurate results in microscale simulations.[8–11] Nie et al.[8] applied the LBM method for MEMS flows and it was shown that LBM can capture behaviors such as velocity slip, nonlinear pressure distribution along the channel and dependance of mass flow rate on Knudsen number[8]. Lim et al. used specular bounce back boundary condition for gas surface interaction for their LBM simulations[9]. Their results for slip flow regime was in good agreement with experimental data for pressure distributions along the microchannel. Zhang et al. showed that LBM can predict the correct trend of mass flow rate as the Knudsen number increases along the microchannel[11].

The purpose of this study is to present statistical simulations of rarefied gas flows in microchannels using both DSMC and LBM methods and demonstrate the performance and accuracy of the methods by comparing with theoretical models. The outline of this paper is presented as follows. First the DSMC and LBM methods are summarized and applicability to MEMS flows are discussed. Next the numerical test case is described and the boundary conditions are specified. The pressure distribution, wall slip velocity and velocity profiles along the channel are presented in the results section.

II. Description of Molecular Models

A. Direct Simulation Monte Carlo (DSMC)

DSMC is a direct particle simulation method, which is based on kinetic theory. The DSMC method has been pioneered by Bird.[2] It is based on employing a number of simulated molecules in order to mimic the motion of relatively larger amount of real molecules. The motion of particles and interactions are then used in order to calculate their new positions, velocities etc while conservation of mass, momentum and energy is satisfied. In DSMC the molecular motions and the intermolecular collisions are uncoupled over small time intervals. Particle motions are modeled deterministically, while the collisions are treated statistically. The base of the DSMC algorithm is made up of four primary processes:

1. Move the particles
2. Index and cross-reference the particles
3. Simulate collisions
4. Sample the flow field.

These processes are uncoupled during each time-step of which the selection is very important since it must be less than the mean collision time. Here each process is summarized briefly:

The first process enforces the boundary conditions and samples macroscopic properties along solid surfaces. In order to model the molecule-surface interactions, it is required to apply the conservation laws to individual molecules which enable DSMC to be extended to include physical effects such as chemical reactions, catalytic walls, radiation etc. The second process is the prerequisite for the following steps where the molecular referencing is performed. The third step is a probabilistic process. Here an appropriate number of

representative collisions between randomly selected pairs of molecules within each cell are performed via a collision modeling technique. The last step involves calculating the macroscopic quantities at the geometric center of each cell using spatial coordinated and velocity components of molecules in a particular cell. DSMC method is explicit and time marching so DSMC results are always unsteady.

B. Pressure boundary conditions for DSMC simulation

In this section, an implicit treatment for the upstream and downstream boundary conditions is presented for the DSMC simulation of low-speed micro-flows. This method was proposed by Liou and Fang[12] and then modified slightly by Wang et al.[13] The pressure value at the inlet and the exit boundaries are kept constant by allowing gas molecules to enter both the upstream and downstream boundaries. The number of the entering molecules, their velocities, and internal energies are determined by the local mean velocities, temperature and number densities at the boundaries at every time step. This procedure is described below:

1. *Implicit velocity distributions for entering molecules*

For an equilibrium gas with a one-dimensional mean flow, the quantities associated with the molecules entering the computational domain from the open boundaries can be determined according to the Maxwellian equilibrium distribution function,

$$f_0 = \frac{\beta^3}{\pi^{3/2}} \exp\left(-\beta^2 \acute{c}^2\right) \tag{1}$$

where $\beta = 1/\sqrt{2RT}$. R denotes the universal gas constant, $\acute{c}$ the thermal speed of molecule, and T gas temperature. Using the Maxwellian distribution function, the number flux of the molecules entering the computational domain can be calculated based on the local temperature and the mean flow velocity. The number flux, F_j, from a boundary cell j at an open boundary can be written as

$$F_j = \frac{n_j}{2\sqrt{\pi}\beta_j} \left[\exp\left(-s_j^2 \cos^2\theta\right) + \sqrt{\pi} s_j \cos\theta \{1 + \mathrm{erf}(s_j \cos\theta)\}\right] \tag{2}$$

where $s_j = U_j \beta_j$, $\beta_j = 1/\sqrt{2RT_j}$. erf represents the error function, n_j the number density of molecules in cell j. T_j and U_j denote the local temperature and the streamwise mean velocity component, respectively. s_j denotes the molecular speed ratio and β_j is related to the thermal scattering. θ is the angle between the velocity vector and normal to the boundary element.

2. *Upstream boundary*

The treatment of upstream pressure boundary is based on the theory of characteristics. The velocity of the incoming molecules are calculated according to

$$(u_{in})_j = u_j + \frac{p_{in} - p_j}{\rho_j a_j}, \quad (v_{in})_j = v_j \tag{3}$$

which was proposed by Wang *et al.*[13] To calculate Eq.(3), the local density, temperature are calculated by

$$\rho_j = n_j m, \quad T_j = \frac{3T_{tr} + \zeta_r T_{rot}}{3 + \zeta_r}, \tag{4}$$

where T_{tr} denotes the translational temperature, T_{rot} the rotational temperature, and ζ_r the number of rotational degree of freedom. The local speed of sound is given by $a_j = \sqrt{\gamma RT}$. The local pressure is found by $p_j = n_j k T_j$, where $k = 1.38 \times 10^{-23} J/K$ is the Boltzmann constant. In Eq.(3), p_{in} is the required pressure value to be set at the inlet boundary.

After calculating the velocity of the incoming molecule, the speed ratio s_j is calculated and if $|s_j| < 10$ then the number flux is calculated according to Eq.(2) where $\theta = 0^\circ$ for the upstream boundary and incoming number density is found by $n_{in} = p_{in}/kT_{in}$.

The number flux F_j is multiplied with the time step and the cell height in order to calculate the number of molecules entering the cell j. If the number of molecules entering the cell is larger than 1 than the acceptance-rejection method by Bird[2] and the Maxwellian distribution function are employed to assign the velocity components of the entering molecule in cell j.

Liou and Fang[12] have proposed a modified version of the acceptance-rejection method for micro scale DSMC simulations which is also followed in this study. For the upstream boundary, the streamwise thermal velocity, $\acute{u}$, of the molecules entering the computational domain should be found in the interval $[-U_j, \infty)$, with a distribution function, $f_{\acute{u}} \propto (\beta\acute{u} + s_j)\exp(-\beta^2\acute{u}^2)$. The maximum of this distribution occurs at $\beta\acute{u} = \{(s_j^2+2)^{1/2} - s_j\}/2$ and the ratio of the probability to the maximum probability is

$$\frac{P}{P_{max}} = \frac{2(\beta\acute{u} + s_j)}{s_j + (s_j^2+2)^{1/2}} \exp\left(\frac{1}{2} + \frac{s_j}{2}\{s_j - (s_j^2+2)^{1/2}\} - \beta^2\acute{u}^2\right). \tag{5}$$

To numerically implement the acceptance-rejection method, the upper limit of ∞ is replaced by a cut-off value of $3C_{mp}$ where $C_{mp} = \sqrt{2RT_j}$ is the local most probable thermal speed of molecules. The thermal speed of the entering molecule is randomly sampled in the interval $[-U_j, 3C_{mp}]$ which can be written as $\acute{u} = a + Rf(b-a)$ where a and b are the lower and upper limits of the distribution. Replacing $a = -U_j$ and $b = 3C_{mp}$ gives

$$\acute{u} = -U_j + R_f(U_j + 3C_{mp}) \tag{6}$$

The resulting streamwise total velocity, $u = U_j + \acute{u}$, is obtained as:

$$u = (U_j + 3C_{mp})R_f \tag{7}$$

where R_f represents a random fraction number. Eq.(7) is used to calculate the value of P/P_{max} given by Eq.(5) and if the value of $|P/P_{max}|$ is greater than the next random fraction R_f the thermal speed $\acute{u}$ is accepted and assigned to the entering molecule. Otherwise, Eq.(6) is used to generate another value of $\acute{u}$ and this process is repeated until $|P/P_{max}| > R_f$. The parallel components of the velocity are calculated as $v = A\cos\theta$ and $w = A\sin\theta$. The value of A, lies between 0 and ∞, and has a distribution function, $f_A = \exp(-\beta^2A^2)$. Using the acceptance-rejection method, the magnitude A, can be written as $A = \sqrt{-lnR_f}C_{mp}$. The value of θ is uniformly distributed between 0 and 2π. That is, $\theta = 2\pi R_f$.

3. Downstream boundary

For sub-sonic, pressure-driven flow the downstream pressure condition can be imposed by using the method of characteristics inspired by a characteristic theory used in continuum CFD.[14] The mean velocity quantities are first determined at the exit boundary column of cells by the following sample average equations

$$U_j = \frac{\sum u_j}{N_j}, \quad V_j = \frac{\sum v_j}{N_j}, \tag{8}$$

while local density and temperature was sampled using Eq.(4). The local value of pressure is calculated by $p_j = n_j k T_j$. The calculated mean quantities are then used to calculate the the number and the velocity distribution of the molecules required to enter the computational domain from the exit boundary. In order to do this, first the exit velocity is calculated by

$$(u_e)_j = u_j + \frac{p_j - p_e}{\rho_j a_j}, \quad (v_e)_j = v_j. \tag{9}$$

Here p_e is the user-defined pressure value at the exit boundary. The exit mean flow velocities (U_e, V_e) are then found by averaging Eq.(9) over the exit boundary. The density at the exit is calculated by

$$(\rho_e)_j = \rho_j + \frac{p_e - p_j}{a_j^2}, \tag{10}$$

which provides the value for the number of molecules entering the exit boundary by $n_e = \rho_e/m$. If the speed ratio $s = |U_e/C_{mp}| < 10$ then the number flux at the exit boundary is calculated according to Eq.(2) where $\theta = 2\pi$ for the exit boundary.

Similar to the implementation of upstream boundary condition, the number flux F_j is multiplied with the time step and the cell height in order to calculate the number of molecules entering the cell j. If the number of molecules entering the cell is larger than 1 than the acceptance-rejection method by Bird[2] and the Maxwellian distribution function are employed to assign the velocity components of the entering molecule in cell j.

According to the modified version of the acceptance-rejection method for micro scale DSMC simulations,[12] for the downstream boundary, the streamwise thermal velocity, $\acute{u}$, of the molecules entering the computational domain should be found in the interval $[-\infty, U_j)$, with a distribution function $f_{\acute{u}} \propto (\beta\acute{u} + s_j)\exp(-\beta^2\acute{u}^2)$. To numerically implement the acceptance-rejection method using, the lower limit of $-\infty$ is replaced by a cut-off value of $-3C_{mp}$. The thermal speed of the entering molecule is randomly sampled in the interval $[-3C_{mp}, U_j]$ which gives

$$\acute{u} = -U_j + R_f(U_j - 3C_{mp}) \tag{11}$$

The resulting streamwise exit total velocity, $u = U_j + \acute{u}$, is obtained as:

$$u = (U_j - 3C_{mp})R_f \tag{12}$$

where R_f represents a random fraction number. Eq.(12) is used to calculate the value of P/P_{max} given by Eq.(5) and if the value of $|P/P_{max}|$ is greater than the next random fraction R_f the thermal speed $\acute{u}$ is accepted and assigned to the entering molecule. Otherwise, Eq.(11) is used to generate another value of $\acute{u}$ and this process is repeated until $|P/P_{max}| > R_f$. The parallel components of the velocity are calculated as $v = A\cos\theta + V_j$, $w = A\sin\theta$. The values of A and θ, are calculated in the same way in the upstream boundary case.

C. Lattice-Boltzmann Method (LBM)

Lattice-Boltzmann method has been applied to many fluid flow problems and was proven to serve as a CFD tool alternative to the methods that solve Navier-Stokes equations such as Finite Volume, Finite Element and Finite Difference methods.[15] LBM has the advantage to handle simulations with arbitrary complex geometries such as flow through porous media, ocean modeling etc. The governing equation is a simplified Boltzmann equation and due to the intrinsic kinetic nature of LBM, it can be used in microscale flow simulations where Knudsen number ($Kn > 0$) is greater than zero.

LBM model used in this study follows the evolution of a number of particles by calculating the direction-specific density functions on a lattice.[16] There are different lattice structures that has been used since the beginning of lattice gas methods.[15] In this work we have used the two dimensional lattice structure called D2Q9 which uses 9 velocitites as given in Fig. 1. The ninth velocity is zero which stands for the particles in rest. The length scale ($1\ lu$) is fixed by the distance between nodes. In Fig. 1 the velocity magnitudes of $\mathbf{e_1}$ to $\mathbf{e_4}$ are $1\ lu/ts$ while the velocities denoted by $\mathbf{e_5}$ to $\mathbf{e_8}$ are $\sqrt{2}\ lu/ts$. The D2Q9 model is used here with single relaxation time, τ.

The procedure of LBM method can be summarized in two steps. First step is the collision step where the direction-specific density distributions are relaxed toward quasi-equilibrium distributions. At the second step, the streaming, the distribution functions are moved to the neighboring nodes. Eqn. (13) gives the Lattice Boltzmann equation with streaming and single relaxation time collision operator which is the BGK (Bhatnagar-Gross-Krook) operator.[17]

$$f_a(\mathbf{x} + \mathbf{e_a}\triangle t, t+1) = f_a(\mathbf{x}, t) - \frac{f_a(\mathbf{x}, t) - f_a^{eq}(\mathbf{x}, t)}{\tau} \tag{13}$$

In Eqn.(13), $\mathbf{x}$ denotes the position vector and a stands for one of the 9 possible directions on the lattice. On the D2Q9 lattice structure, the components of the equilibrium distribution function f_a^{eq} are given by the equation

$$f_a^{eq}(\mathbf{x}) \quad = \quad w_a\rho(\mathbf{x})\left[1 + 3\frac{\mathbf{e}_a \cdot \mathbf{u}}{c^2} + \frac{9}{2}\frac{(\mathbf{e}_a \cdot \mathbf{u})^2}{c^4} - \frac{3}{2}\frac{\mathbf{u^2}}{c^2}\right] \tag{14}$$

where $a = 1, \ldots 9$. The weights w_a are $4/9$ for $a = 9$, $1/9$ for $a = 1-4$ and $1/36$ for $a = 5-8$. The macroscopic density and velocity of particles at $\mathbf{x}$ is found by Eq.(15) given below.

$$\rho(\mathbf{x}) = \sum_a f_a(\mathbf{x}), \quad \mathbf{u} = \textstyle\sum_a \frac{\mathbf{e_a f_a(x)}}{\rho(\mathbf{x})} \tag{15}$$

The LBM simulation is initialized by assigning a value for f_a at all lattice nodes in the domain, then the effects of boundary conditions and forces (if any) are incorporated. Finally, the equilibrium distributions are recomputed by Eq. (14), and the macroscopic flow properties are calculated at the next time step using Eq. (15).

For nearly incompressible flows the D2Q9 model is used with single relaxation time ($\tau = 1$) however for rarefied gas flow in microgeometries compressibility effects must be taken into account that is why the relaxation time has to be modified.[8] In this work, the dimensionless relaxation parameter τ in Eq. 13 has been replaced with τ' according to Nie et al.[8]

$$\tau' = \frac{1}{2} + \frac{1}{\rho}(\tau - \frac{1}{2}). \tag{16}$$

For boundary conditions on the wall surfaces the bounce-back boundary condition is coupled with specular reflection using a reflection coefficient r_b as presented by Tang et al.[18]. r_b represents the proportion of bounce-back reflections while $(1 - r_b)$ represents the specular reflections on the solid nodes. $r_b = 1$ corresponds to pure bounce-back reflection where $r_b = 0$ gives a pure specular reflection. In our simulations the value of r_b was selected to match the velocity profiles given by DSMC and theoretical results. The boundary conditions of bottom and top walls can be viewed as:

$$\begin{aligned}
f_2(x,1) &= f_4(x,1) \\
f_5(x,1) &= r_b f_7(x,1) + (1-r_b) f_8(x,1) \\
f_6(x,1) &= r_b f_8(x,1) + (1-r_b) f_7(x,1) \\
f_4(x,Ly) &= f_4(x,Ly) \\
f_7(x,Ly) &= r_b f_5(x,Ly) + (1-r_b) f_6(x,Ly) \\
f_8(x,Ly) &= r_b f_6(x,Ly) + (1-r_b) f_5(x,Ly).
\end{aligned} \tag{17}$$

At the inlet and exit of the microchannel pressure boundary conditions are assigned following.[19] The specular/bounceback reflection was omitted at top and bottom corner nodes at inlet and exit boundaries.

III. Results and Discussion

In this section, isothermal microchannel flows in two dimensions are investigated using DSMC and LBM methods. A microchannel with aspect ratio ($L/h = 20$) is used with inlet to exit pressure ratio $1.84 < \Pi < 4.14$. The working gas is Nitrogen and the Knudsen number at the exit is $Kn_o = 0.127$ for the slip flow case and $Kn_o = 0.255$ for the transition flow case.

For the DSMC simulations, the geometry of the microchannel used was $H = 0.2m$ and $L = 4m$. The flow domain was discretized with 200 cells in the flow direction and 120 across the channel where a total of $960,000$ molecules were simulated. The time step used was $dt_{DSMC} = 2 \times 10^{-6} s$ and the total number of samples is $10,200$. The pressure at the inlet and exit boundaries were fixed at constant pressure values using the method described in Section(B). In order to illustrate the significance of correct boundary conditions on the solution, the DSMC results obtained with pressure and velocity boundary conditions are compared in Fig. (3). For the DSMC simulation with velocity inlet boundary condition, a value of $25m/s$ uniform velocity was assigned at the inlet with the number density $8 \times 10^{19} 1/m^3$ and the temperature $300K$. The corresponding pressure conditions were $p_{in} = 0.58\ Pa$ and $p_e = 0.21\ Pa$ at the inlet and exit respectively. It was observed that the new boundary conditions enable to keep the inlet and exit pressure and density values at the desired level throughout the simulation. The deviation of temperature from the freestream value of 300 K is found to be less with the new boundary implementation. The flow rate has been tracked at the inlet, center and exit of the channel and the values have converged to the same value as seen in Fig. (3).

For the simulations with LBM, channel length was $L_{LBM} = 200lu$ and channel width was $H_{LBM} = 10lu$ so the aspect ratio was $L_{LBM}/H_{LBM} = 20$. The inlet and exit the density is set to match the same pressure ratio used in the DSMC simulations. The Knudsen number in LBM was calculated by,

$$Kn = \frac{a(\tau - 0.5)}{\rho H}, \tag{18}$$

which was proposed by Nie *et al.*[8]. The coefficient $a = 0.835$ is specified in order to match with the DSMC data. It was observed that Eq.(18) captures the Knudsen number variation along the centerline of the microchannel correctly both in slip flow (Fig.4(a)) and transition regime (Fig.4(b)).

Fig.5(a) and Fig.6(a) show the DSMC and LBM results for pressure distribution along the channel normalized with exit pressure for the slip and transition flow case at various pressure ratios. The pressure distribution is nonlinear as expected for a compressible channel flow. However the LBM method predicts a larger deviation from linearity compared to DSMC simulation as seen in Fig. (5(b), 6(b)) especially for the $\Pi = 4.14$ case. The dashed line is the Navier-Stokes based analytical solution of Arkilic et al.[20] which is valid in the slip flow regime and calculated as

$$\tilde{p}(x) = -6\sigma Kn_o + \sqrt{(6\sigma Kn_o)^2 + (1 + 12\sigma Kn_o)\tilde{x} + (\Pi^2 + 12\sigma Kn_o\Pi)(1 - \tilde{x})}. \tag{19}$$

It was observed that both DSMC and LBM methods predict that the non-linearity of pressure distribution reduces as the Knudsen number increases (Fig.5(b) and Fig.6(b)). This behavior confirms previous findings that the effect of compressibility reduces as the flow becomes more rarefied.[21]

Velocity profiles for $1.84 < \Pi < 4.14$, normalized with the local maximum velocity at three different x/L locations are shown in Fig.(7(a)–7(c)) and Fig.(8(a)–8(c)). The velocity profiles obtained by both methods are parabolic and are observed to be in good agreement. Both methods show that the slip velocity on the wall increases in the axial direction. The continuum-based analytical solution for the velocity profile using the 2^{nd} order slip-boundary condition by Beskok et al.[21] can be written as

$$\frac{u}{u_c} = \left[-\left(\frac{y}{H}\right)^2 + \frac{y}{H} + \frac{Kn_o}{1 + Kn_o} \right] / \left(\frac{1}{4} + \frac{Kn_o}{1 + Kn_o} \right) \tag{20}$$

which is also plotted in Fig.(7(a)–7(c)) and Fig.(8(a)–8(c)). DSMC method handles the particle-wall interactions more accurately that is why the tangential slip along the walls is well captured. It was observed that the DSMC results with pressure boundary conditions agree well with the the analytical prediction for the velocity profile along the channel at different local Knudsen numbers. In the slip flow case, using a value of $r_b = 0.6$ for the bounce-back reflection coefficient, velocity profiles obtained with the LBM method match the DSMC and analytical data perfectly. In the transition flow case, the value of r_b was increased to $0.7 - 0.85$.

IV. Conclusion

In this study, the microchannel flow with pressure boundary conditions specified at the inlet and exit are simulated using DSMC and LBM methods. The pressure distribution was found to be nonlinear due to the compressibility effects in microchannels. The rarefaction is indicated by the local Knudsen number variation along the channel captured accurately bu both methods which was observed to be between $0.03 < Kn < 0.125$ for the slip flow case and $0.06 < Kn < 0.255$ for the transition flow case. The velocity profiles plotted at different cross sections along the channel showed slip-flow at the surfaces is a result of rarefaction.

References

[1]GadelHak, M., "The Fluid Mechanics of Microdevices – The Freeman Scholar Lecture," *Journal of Fluids Engineering*, Vol. 121, 1999, pp. 5–33.

[2]Bird, G., A., *Molecular Gas Dynamics and the Direct Simulation of Gas Flow*, Clarendon Press, Oxford, U.K., 1994.

[3]Chen, C.-S., "Numerical Method for Predicting Three-dimensional Steady Compressible Flow in Long Microchannels," *Journal of Micromechanics and Microengineering*, Vol. 14, 2004, pp. 1091–1100.

[4]Guo, Z. Y. and Wu, X. B., "Compressibility Effect on the Gas Flow and Heat Transfer in a Microtube," *International Journal of Heat and Mass Transfer*, Vol. 40, No. 13, 1997, pp. 3251–3254.

[5]Xue, H., Fan, Q., and Shu, C., "Prediction of Micro-Channel Flows Using Direct Simulation Monte Carlo," *Probabilistic Engineering Mechanics*, Vol. 15, 2000, pp. 213–219.

[6]Fang, Y. and Liou, W. W., "Computations of the Flow and Heat Transfer in Microdevices Using DSMC with Implicit Boundary Conditions," *ASME Journal of Heat Transfer*, Vol. 124, April 2002, pp. 338–345.

[7]Wang, M. and Li, Z., "Nonideal Gas Flow and Heat Transfer in Micro- and Nanochannels Using the Direct Simulation Monte Carlo Method," *Pyhsical Review E*, Vol. 68, No. 046704, 2003.

[8]Nie, X., Doolen, Gary, D., and Chen, S., "Lattice-Boltzmann Simulations of Fluid Flow in MEMS," *Journal of Statistical Pyhsics*, Vol. 107, 2002, pp. 279–289.

[9]Lim, C., Shu, C., Niu, X., and Chew, Y., "Application of lattice Boltzmann method to simulate microchannel flows," *Physics of Fluids*, Vol. 14, No. 7, 2002, pp. 2299 – 2308, Microflows;.

[10]Lee, T. and Lin, C.-L., "Rarefaction and compressibility effects of the lattice-Boltzmann-equation method in a gas microchannel," Vol. 71, No. 4, 2005, pp. 046706 – 1.

[11]Zhang, Y., Qin, R., and Emerson, David, R., "Lattice Boltzmann simulation of rarefied gas flows in microchannels," *Physical Review E - Statistical, Nonlinear, and Soft Matter Physics*, Vol. 71, No. 4, 2005.

[12]Liou, W. and Fang, Y., "Implicit boundary conditions for direct simulation Monte Carlo method in MEMS flow predictions," *CMES-Computer Modeling in Engineering & Sciences*, Vol. 1, No. 4, 2000, pp. 119 – 128.

[13]Wang, M. and Li, Z., "Simulations for gas flows in microgeometries using the direct simulation Monte Carlo method," *International Journal of Heat and Fluid Flow*, Vol. 25, No. 6, 2004, pp. 975 – 985.

[14]Whitfield, D. L. and Janus, J. M., "Three-dimensional unsteady Euler equations solution using flux vector splitting." *AIAA Paper*, 1984.

[15]Succi, S., *The Lattice Boltzmann Equation for Fluid Dynamics and Beyond*, Clarendon Press, Oxford, U.K., 2001.

[16]Sukop, M. and Or, D., "Lattice Boltzmann Method for Modeling Liquid-Vapor Interface Configurations in Porous Media," *Water Resources Research*, Vol. 40, Jan. 2004, Art. No. W01509.

[17]Bhatnagar, P., Gross, E., and Krook, M., "A Model for Collision Processes in Gases. I. Small Amplitude Processes in Charged and Neutral One-component Systems," *Pyhsical Review*, Vol. 94, No. 3, 1954, pp. 511–525.

[18]Tang, G., H., Tao, W., Q., and He, Y., L., "Gas flow study in MEMS using lattice Boltzmann method," *International Conference on Microchannels and Minichannels*, Vol. 1, 2003, pp. 389 – 396.

[19]Zou, Q. and He, X., "On pressure and velocity boundary conditions for the lattice Boltzmann BGK model," *Physics of Fluids*, Vol. 9, No. 6, 1997, pp. 1591 –.

[20]Arkilic, E., B., Schmidt, M., A., and Breuer, K., S., "Gaseous slip flow in long microchannels," *Journal of Microelectromechanical Systems*, Vol. 6, No. 2, 1997, pp. 167 – 178.

[21]Karniadakis, G. and Beskok, A., *Micro Flows: Fundamentals and Simulation*, Springer-Verlag, NY, U.S.A, 2001.

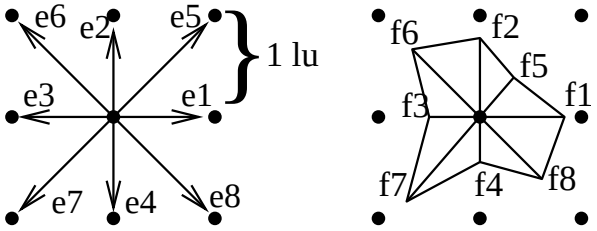

Figure 1. (a) D2Q9 lattice. (b) An example of direction specific density distribution function f.

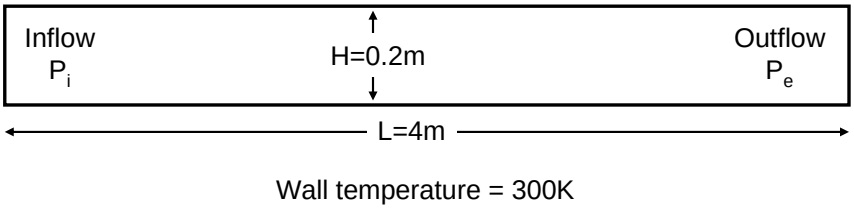

Figure 2. Channel geometry. (Dimensions not to scale.)

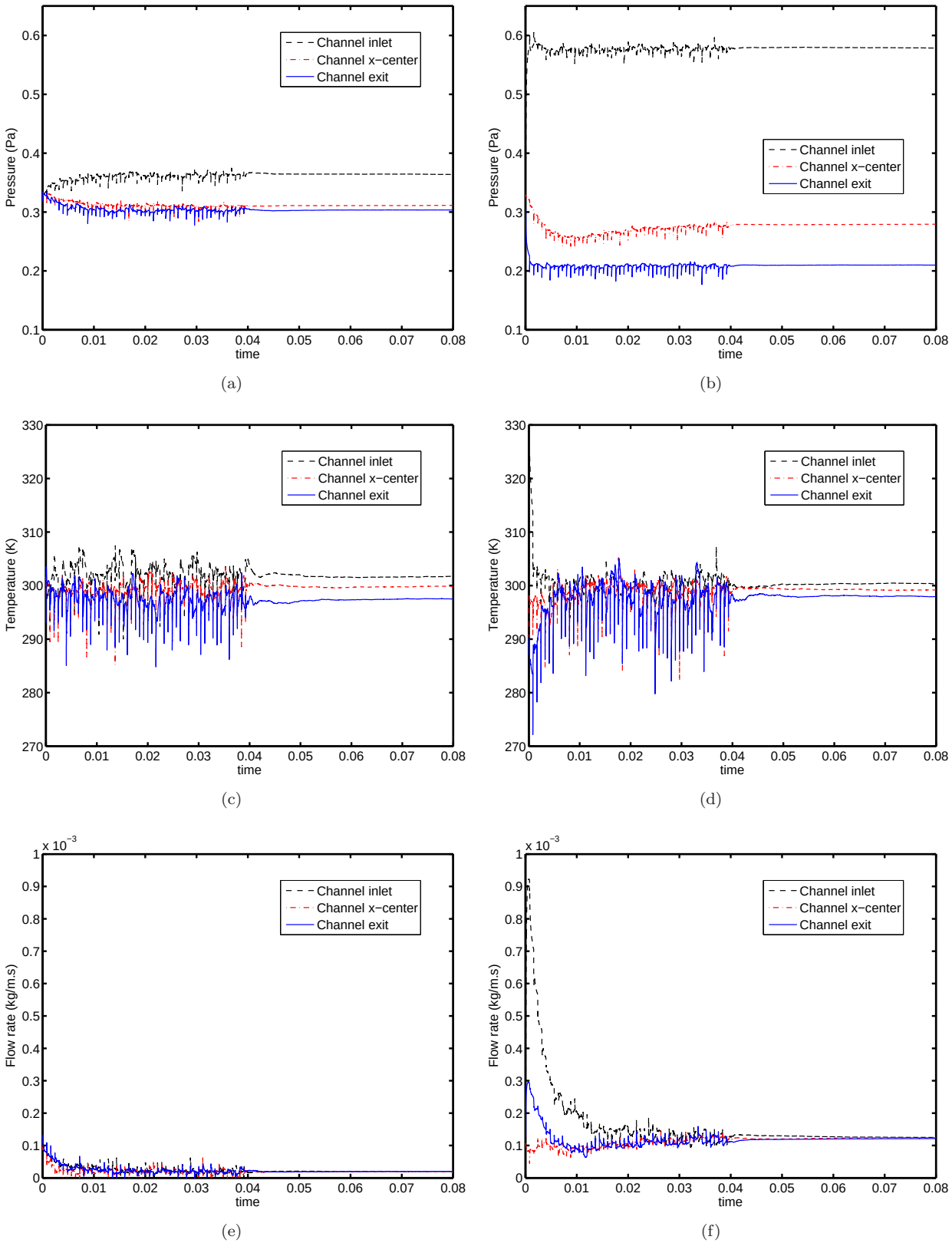

Figure 3. Evolution of the average value of flow properties at the upstream and downstream boundaries calculated by (left column) velocity boundaries (right column) pressure boundaries.

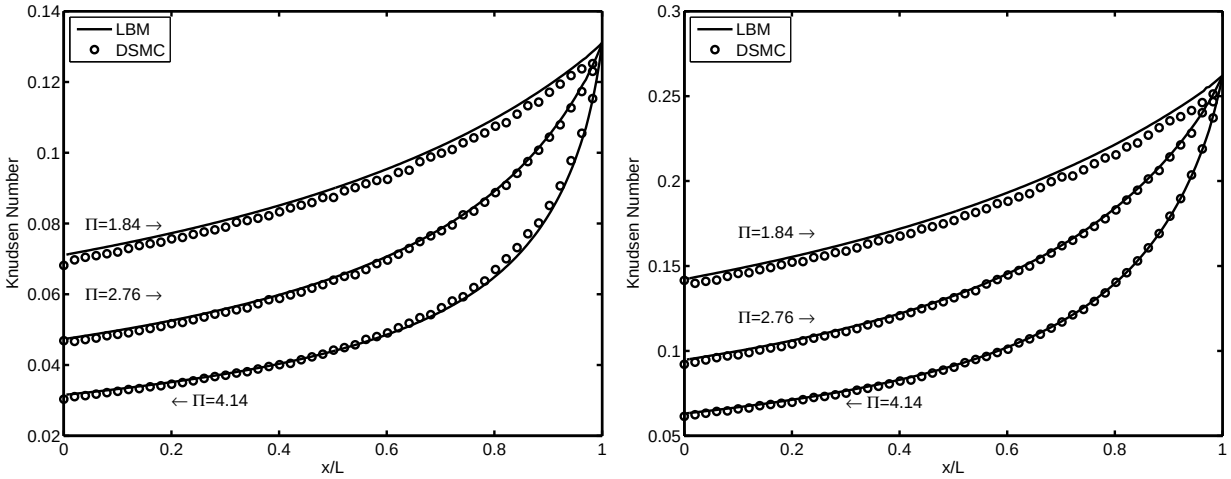

Figure 4. Knudsen number along the channel as calculated by the LBM and DSMC simulations.(a) Slip flow regime (b) Transition flow regime.

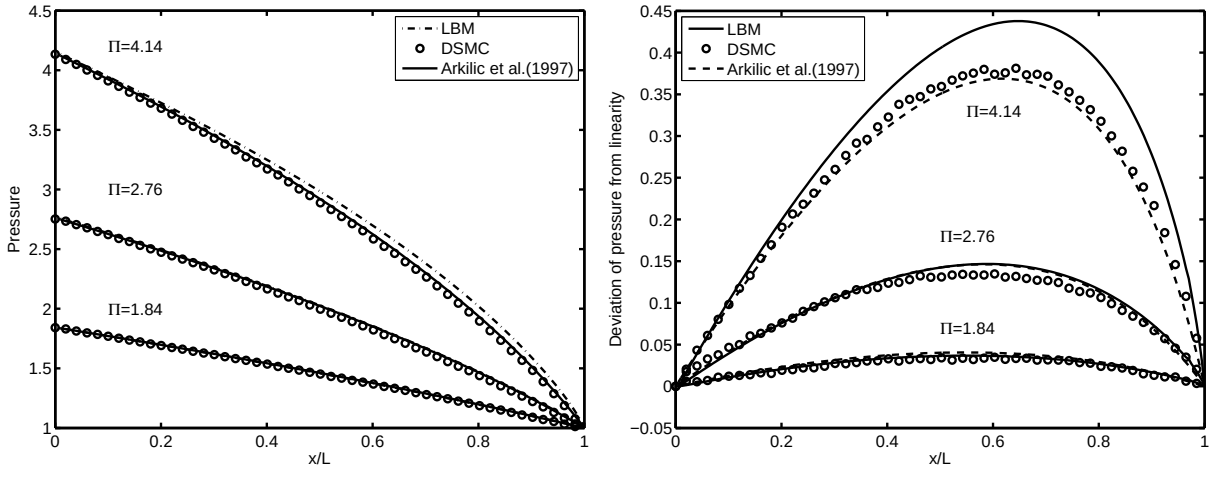

Figure 5. (a)Centerline pressure distribution along the channel as predicted by the LBM and DSMC simulations in the slip regime. (b) Deviation from linearity.

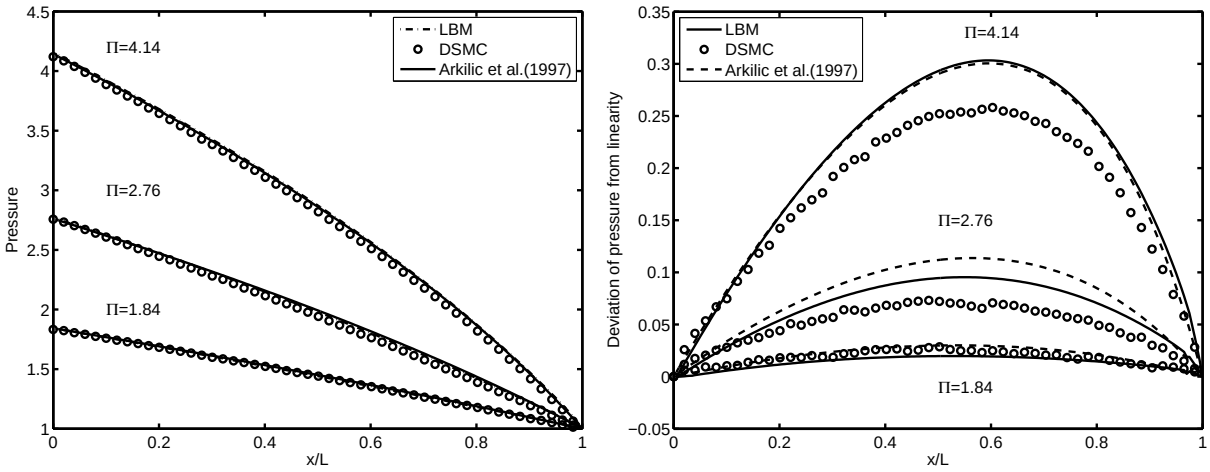

(a) (b)

Figure 6. (a)Centerline pressure distribution along the channel as predicted by the LBM and DSMC simulations in the transition regime. (b) Deviation from linearity.

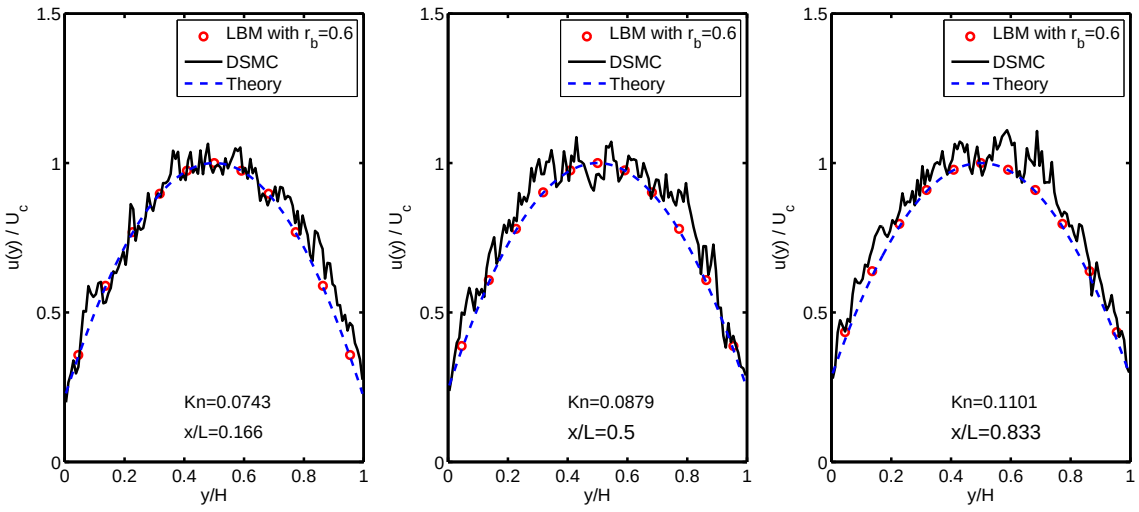

(a) $Kn_o = 0.12, \Pi = 1.84$

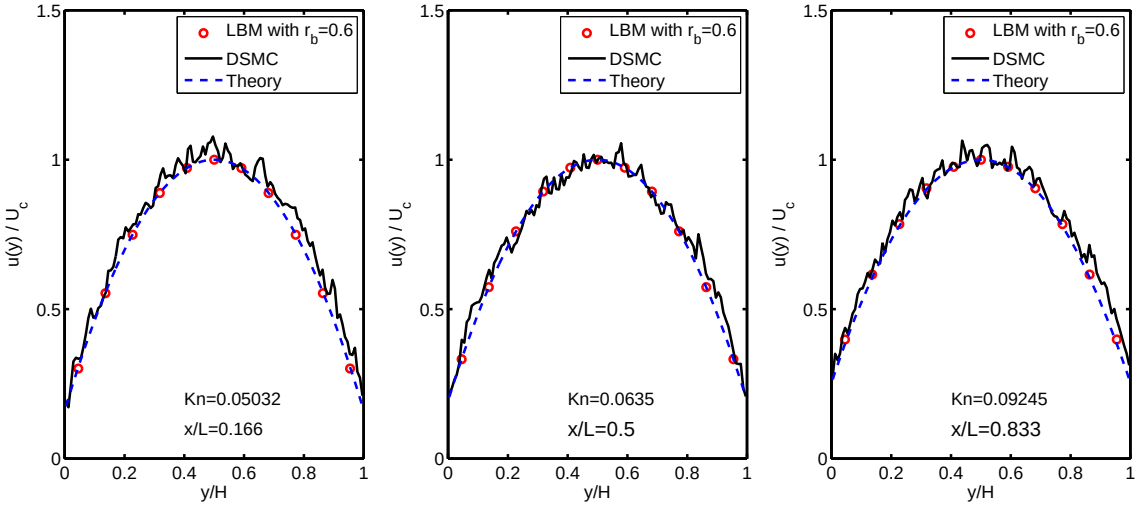

(b) $Kn_o = 0.12, \Pi = 2.76$

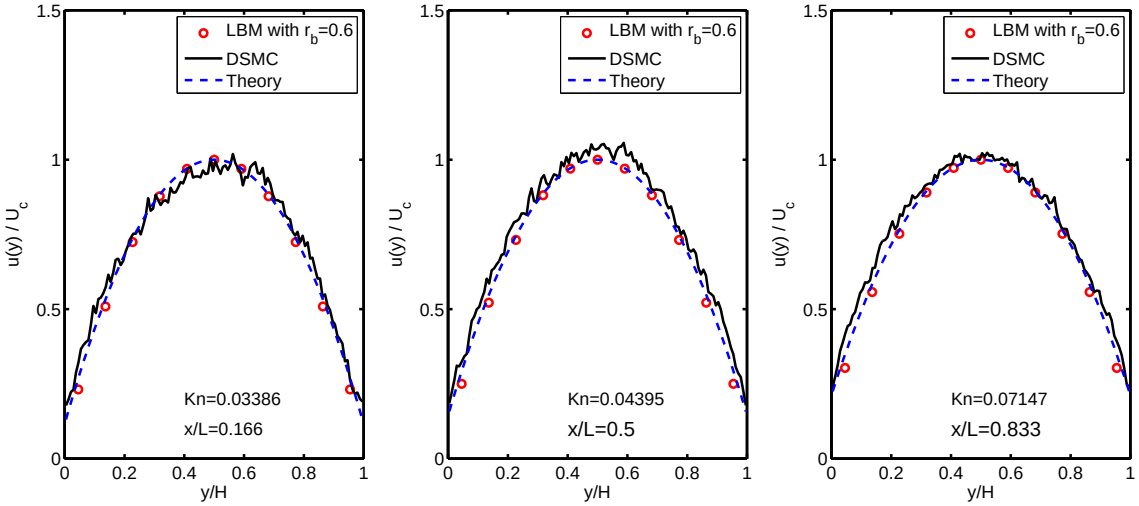

(c) $Kn_o = 0.12, \Pi = 4.14$

Figure 7. Velocity profiles predicted by the LBM and DSMC simulations at various x/L locations for the slip flow case.

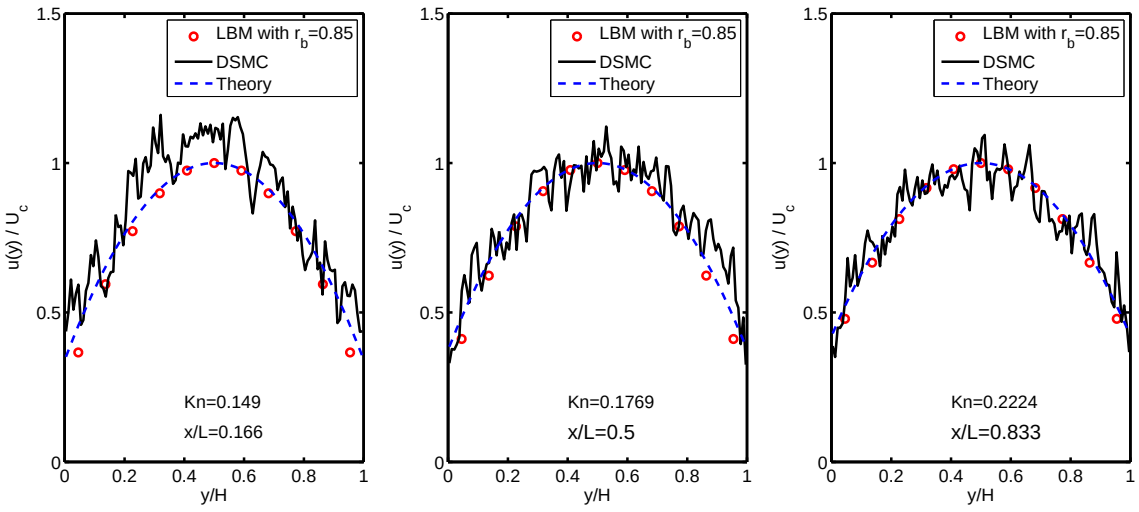

(a) $Kn_o = 0.255, \Pi = 1.84$

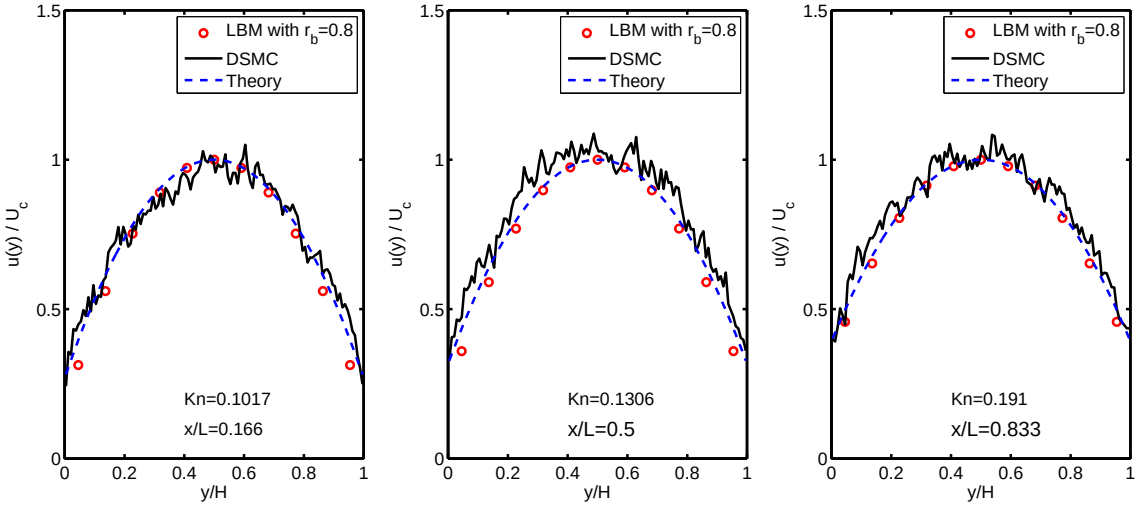

(b) $Kn_o = 0.255, \Pi = 2.76$

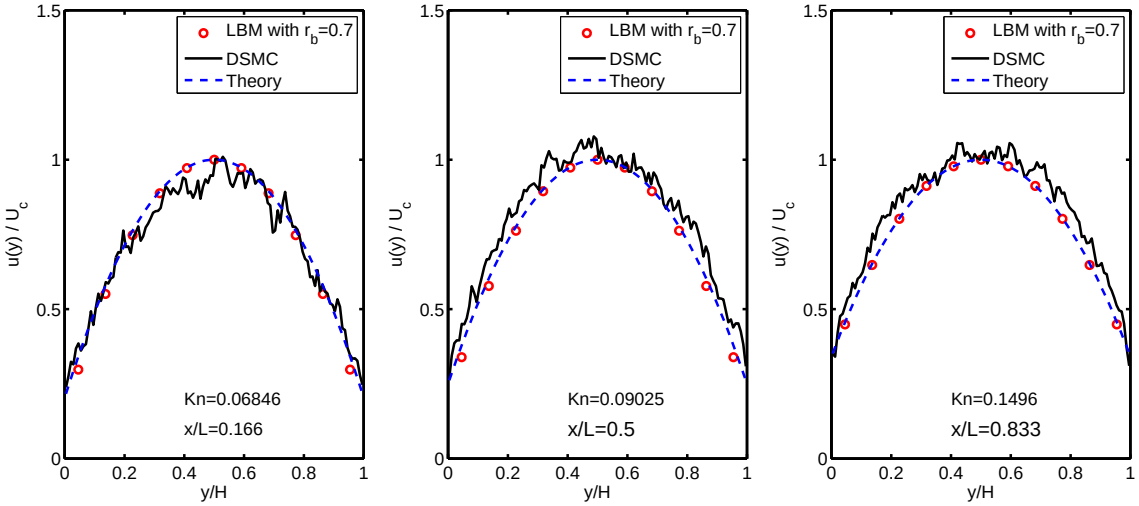

(c) $Kn_o = 0.255, \Pi = 4.14$

Figure 8. Velocity profiles predicted by the LBM and DSMC simulations at various x/L locations for the transition flow case.